Thermodynamic Models for the Temperature and Pressure Variations Within Adiabatic Caverns of Compressed Air Energy Storage Plants

R. Kushnir

A. Ullmann[1]
e-mail: ullmann@eng.tau.ac.il

A. Dayan

Department of Fluid Mechanics and Heat Transfer,
School of Mechanical Engineering
Tel Aviv University,
Tel Aviv 69978 Israel

The temperature and pressure variation limits within the cavern of a compressed air energy storage (CAES) plant affect the compressor and turbine works, the required fuel consumption and therefore the overall plant performance. In the present work, the thermodynamic response of adiabatic cavern reservoirs to charge/discharge cycles of CAES plants are studied. Solutions for the air cavern temperature and pressure variations were derived from the mass and energy conservation equations, and applied to three different gas state equations, namely, ideal, real, and a self-developed simplified gas models. Sensitivity analyses were conducted to identify the dominant parameters that affect the storage temperature and pressure fluctuations. It is demonstrated that a simplified gas model can adequately represent the air thermodynamic properties. The stored air maximal to minimal temperature and pressure ratios were found to depend primarily on, both the ratio of the injected to the initial cavern air mass, and the reservoir mean pressure. The results also indicate that the storage volume is highly dependent on the air maximum to minimum pressure ratio. Its value should preferably be in between 1.2 and 1.8, where the exact selection should account for design and economic criteria. [DOI: 10.1115/1.4005659]

Keywords: compressed air energy storage (CAES), underground storage, cavern reservoirs, thermodynamic modeling

1 Introduction

Incorporation of energy storage facilities in the electrical power industry can reduce, both pollution and fossil fuel depletion, and yet be economical. Energy storage systems should effectively transfer excess energy of base load units during low demand periods to periods of high demand. This utilization of off-peak electrical power reduces the fossil fuel consumption of higher heat rate peaking systems and improves the capacity factor of the efficient base load units. In this respect, CAES is an advantageous alternative for supplying peaking power to electric utilities. A CAES plant provides the benefit of compressing air during off peak hours to an underground reservoir at the low cost of excess base-load electrical power. During peak hours, the compressed air is released and fired to drive the expansion stages of gas turbines. The compressed air can be stored in three geological types of underground reservoirs: salt caverns, hard rock caverns, and porous reservoirs (such as depleted gas reservoirs or aquifers [1,2]). The changes in temperature and pressure of the reservoir stored air (caused by cyclical air injections and withdrawals) are essential factors to be considered in the design of the storage plant. For a given set of operating conditions, the required storage volume and the number of wells (for porous reservoirs) are affected by those fluctuations. Furthermore, the selection of the compression equipment is one that must meet the maximal storage pressure, whereas the minimum storage pressure essentially determines the turbine inlet pressure.

The present study addresses the air storage in cavern reservoirs. To date, there are two operational CAES plants in the world: the 290 MW plant at Huntorf, Germany, built in 1978 [3], and the 110 MW plant in McIntosh, Alabama, commissioned in 1991 [4]. Both plants are using solution mining salt caverns as their underground reservoir. Although, a considerable amount of studies on CAES exist, only few consider the temperature and pressure aspects of CAES reservoirs. Within them are the models developed by the constructors of the two existing CAES plants. Their publications, however, contain only results related to the specific operation of the Huntorf and McIntosh plants and do not provide mathematical formulations [5–7]. Essentially, the models are based on mass and energy conservation and account for heat transfer through the caverns walls but lack any details on the thermodynamic assumptions upon which the models were developed. Separately, the temperature changes in cavern reservoirs were treated by Osterle [8], who preformed a thermodynamic analysis of CAES based on the first and second laws. The air was considered to be an ideal gas and the cavern to be adiabatic. Solution for the air temperature was obtained for the cavern pressurization from a minimum to a maximum pressure, and back to the minimum. The results show that following a series of charge/discharge cycles, the reservoir maximum and minimum temperatures approach asymptotic limits (i.e., steady periodic conditions). Skorek and Banasiak [9] performed thermodynamic analyses of CAES systems, which included cavern temperature and pressure calculations for a steady charge/discharge cycle. They incorporated the assumptions of semi-ideal gases and adiabatic cavern walls. It should be noted that both Refs. [8] and [9] focused their analyses on the modeling of the entire power plant, where limited attention was provided to the reservoir thermodynamic response. Nonetheless, their results for specific conditions are examined and used for comparison in the current study.

[1]Corresponding author.

Contributed by the Advanced Energy Systems Division of ASME for publication in the JOURNAL OF ENERGY RESOURCES TECHNOLOGY. Manuscript received September 1, 2010; final manuscript received November 4, 2011; published online March 16, 2012. Assoc. Editor: Srinivas Katipamula.

In this work, the thermodynamic characteristics of adiabatic reservoir response to charge/discharge cycles of CAES plants are studied. It includes the exploration of the cavern temperature and pressure variations, which are an essential component of the plant capacity and operational design. Though heat transfer through the caverns walls may have an influencing role, the study of adiabatic reservoirs has merit for several reasons. First, it provides a reference solution, which is a limiting case for conditions of negligible heat transfer through the caverns walls. Second, it offers clear analytical solutions that shed light on the thermodynamic behavior of the air during cycle phases of compression, storage, and discharge. Furthermore, it provides a tool to examine and choose the most suitable thermodynamic state equation of air that yields a representative model that is easy to use. Adoption of more accurate equations of state has merit, provided that it does not overly complicate the model utilization. In this respect, a simple and more accurate model paves a preferred path toward the extension of the model to account for heat transfer phenomena, as well as for comparison of results against test data.

In principle, a CAES system can operate in several ways. The compressor train may work with a constant outlet pressure, which implies that the air mass flow rate is being reduced during operation. Alternatively, the air compression may supply a constant mass flow rate, which entails an increasing outlet pressure. Pressure changes in the latter case and flow rate changes in the former are subject to the underground storage physical characteristics. Theoretically, the compressor can work in a third way which matches its characteristics and where both the outlet pressure and mass flow rate would vary accordingly. These different ways of operations also apply to the discharge stage.

The Huntorf and the McIntosh plants operate with constant air mass flow rates, through both, the compressor and turbine machinery. This form of operation defines the plant design requirements so as to maintain a reservoir air mass balance. In addition, it provides a steady turbine operation through the throttling of the discharged air to a fixed pressure. The throttling pressure loss is easily offset by the high turbine efficiency gained by this mode of operation. Therefore, the current research is focused on that type of operation. Solutions for the reservoir temperature and pressure variations were developed for the aforementioned realistic operating conditions; namely, two periods of constant mass flow rate, one for the charging phase and the other for the discharge, and zero flow in between. It is also assumed that the air is cooled to a certain temperature (by an after-cooler) prior to storage. The developed model can be applied to any set of such operating condition required by the above-ground facilities.

2 Formulation of the Problem

Consider a cavern reservoir of constant volume V, located at a certain distance below the surface, as shown in Fig. 1. Initially, the cavern contains compressed air at a pressure P_0 and temperature T_0 (equaling surrounding rock temperature). During a CAES plant operation air flows into and out of the cavern cyclically at quasi-equilibrium conditions (relatively slow process). Upon considering the cavern port and walls as the boundaries of a control volume (see Fig. 1), and applying the mass and energy conservation equations, subject to the generalized gas state equation, one obtains

$$V\frac{d\rho}{dt} = (F_i(t) + F_e(t))\dot{m}_c \tag{1}$$

$$V\frac{d(\rho e)}{dt} = F_i(t)\dot{m}_c\left(h_i + \frac{v_i^2}{2} + gz_i\right) + F_e(t)\dot{m}_c\left(h_e + \frac{v_e^2}{2} + gz_e\right) \tag{2}$$

$$p = \mathbf{Z}\rho\mathbf{R}\mathrm{T} \tag{3}$$

where e is the specific energy of the cavern air

$$e = u + \frac{v^2}{2} + gz \tag{4}$$

u and h are the specific internal energy and enthalpy, and $v^2/2$ and gz are the kinetic and potential energies per unit mass (where z is a vertical coordinate), respectively. The subscript i denotes the control volume inlet air conditions and the subscript e designates the outlet air conditions. p, ρ, and T, which represent the instantaneous pressure density and temperature of the air within the cavern, are assumed to be uniform throughout the storage space. This is a reasonable assumption owing to both air circulation and slow rates of temperature variations. The product $(F_i(t)+F_e(t))\dot{m}_c$ represents the momentary air mass flow rate at the cavern port, where $\dot{m}_c$ is the compressor flow rate, and the sum $F_i(t)+F_e(t)$ is a dimensionless periodic function with a cycle time t_p. Figure 2 shows the variations of $F_i(t)+F_e(t)$ of a CAES plant operating with compressor and turbine constant mass flow rates. The indicated time intervals are: t_1 for the charging time, $t_2 - t_1$ for the storage time, $t_3 - t_2$ for the power generation time, and **CD** represents the discharging to charging mass flow ratio (equal also to the ratio of the charging time to discharging time). Accordingly, the functions $F_i(t)$ and $F_e(t)$ are defined as

$$F_i(t) = \begin{cases} 1 & (n-1)t_p \le t \le (n-1)t_p + t_1 \\ 0 & \text{otherwise} \end{cases},$$
$$F_e(t) = \begin{cases} -\mathbf{CD} & (n-1)t_p + t_2 \le t \le (n-1)t_p + t_3 \quad n = \text{Cycle number} \\ 0 & \text{otherwise} \end{cases} \tag{5}$$

Equations (1) and (2) stand for adiabatic and impermeable control volume boundaries. Additionally, during the charging stage, the air entering the cavern is at the cavern pressure and at a constant temperature T_i (which not necessarily equal to the after-cooler temperature). The air leaving the cavern during the discharge stage has the cavern pressure and temperature. Equation (2) is rearranged according to the thermodynamic state principle, for which two independent intensive properties are sufficient to define the state of a simple compressible system, hence

$$\frac{d(\rho e)}{dt} = \rho\frac{du}{dt} + e\frac{d\rho}{dt} = \rho c_v\frac{dT}{dt} + \left[\rho\left(\frac{\partial u}{\partial \rho}\right)_T + e\right]\frac{d\rho}{dt} \tag{6}$$

where c_v is the constant volume specific heat of the air. Note that the variation of the velocity with time is negligible and therefore $de/dt \cong du/dt$. The substitution of Eqs. (1), (3), (4), and (6) into Eq. (2) yields

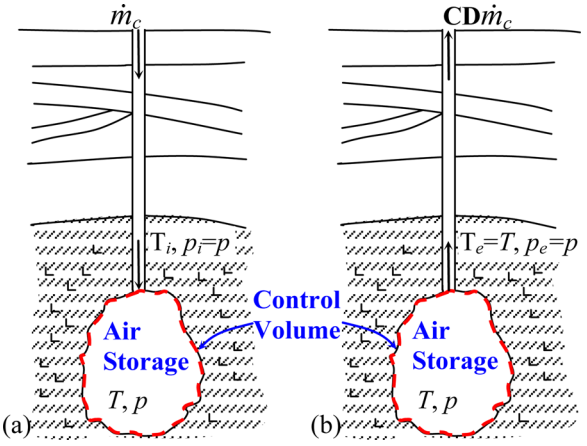

Fig. 1 Schematics of an underground air storage cavern: (*a*) during charge; (*b*) during discharge

$$V\rho c_v \frac{dT}{dt} = F_i(t)\dot{m}_c\left(h_i - h + \mathbf{ZR}T - \rho\left(\frac{\partial u}{\partial \rho}\right)_T + \frac{v_i^2}{2} + g\Delta z\right) + F_e(t)\dot{m}_c\left(\mathbf{ZR}T - \rho\left(\frac{\partial u}{\partial \rho}\right)_T + \frac{v_e^2}{2} + g\Delta z\right) \tag{7}$$

where $\Delta z \equiv (z_i\text{-}z)=(z_e\text{-}z)$. From thermodynamic properties relationships, one gets

$$\left(\frac{\partial u}{\partial \rho}\right)_T = -\frac{\mathbf{R}T^2}{\rho}\left(\frac{\partial \mathbf{Z}}{\partial T}\right)_\rho \tag{8}$$

$$h = h^0 + \mathbf{R}T(\mathbf{Z}-1) - \int_0^\rho \frac{\mathbf{R}T^2}{\rho}\left(\frac{\partial \mathbf{Z}}{\partial T}\right)_\rho d\rho \tag{9}$$

$$c_v = c_p^0 - \mathbf{R} - \mathbf{R}\int_0^\rho \left[T^2\left(\frac{\partial^2 \mathbf{Z}}{\partial T^2}\right)_\rho + 2T\left(\frac{\partial \mathbf{Z}}{\partial T}\right)_\rho\right]\frac{d\rho}{\rho} \tag{10}$$

where

$$h^0 = h^0_{\text{ref}} + \int_{T_{ref}}^T c_p^0 dT \tag{11}$$

c_p^0 is the isobaric specific heat of the air at low density (ideal gas), T_{ref} is a selected reference temperature, and h^0_{ref} is the air enthalpy at low density and temperature T_{ref}. For any given compressibility factor $\mathbf{Z}(\rho,T)$ and specific heat $c_p^0(T)$, Eq. (7) can be solved for the cavern air temperature during plant operation, which in turn can be substituted into Eq. (3) to obtain the cavern air pressure.

It should be noted that for practical conditions, both the kinetic and potential energies terms of Eq. (7) are negligible. For example, the maximum velocity at the Huntorf plant well is 20 m/s (to assure stability [5]), and the caverns are 150 m in height (i.e., $\Delta z = 75$ m). The kinetic and potential energies terms are, therefore, 0.2 and 0.74 kJ/kg, respectively. For a typical temperature and pressure of 300 K and 45 bar, the "specific pressure energy" term p/ρ ($=\mathbf{ZR}T$) is 85.4 kJ/kg and the term $-\rho(\partial u/\partial\rho)_T$ is about 9 kJ/kg. Therefore, the omission of the kinetic and potential energies from the governing equations is justified (discussed also in Sec. 4.1).

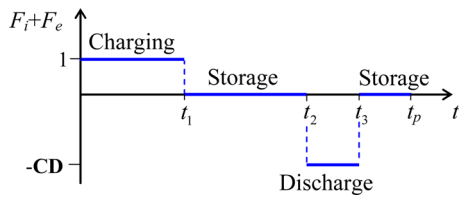

Fig. 2 The dimensionless air mass flow-rate at the cavern port during a CAES plant cycle

3 Solutions for Several Thermodynamic Property Models

Solutions for the cavern air temperature and pressure are dependent on the air thermodynamic properties. In this section, three different thermodynamic state equations of air are presented, namely, the ideal gas model, a self-developed simplified real gas model, and a complex real gas model (Sychev et al. [10]). It is demonstrated that under practical conditions, it is sufficient to represent the thermodynamic properties by the simplified real gas model.

3.1 Ideal Gas Model. The simplest solution is obtained by considering the air to be an ideal gas. Additionally, for moderate ranges of temperature variations, it is reasonable to assign a constant value to either specific heat, hence

$$\mathbf{Z} = 1, \quad c_p^0 = c_{p0}^0, \quad c_v = c_{v0}^0 = c_{p0}^0 - \mathbf{R} \tag{12}$$

where c_{p0}^0 and c_{v0}^0 are the air specific heats at the initial temperature T_0. Under such conditions and for negligible kinetic and potential energies, Eq. (7) is reduced to

$$\frac{V\rho c_{v0}^0}{\dot{m}_c}\frac{dT}{dt} = F_i(t)\left(c_{p0}^0(\mathrm{T}_i - T) + \mathbf{R}T\right) + F_e(t)\mathbf{R}T \tag{13}$$

The ideal gas model leads to a simple linear differential equation which can easily be solved analytically for the air temperature in the cavern. The first cycle cavern air density, temperature, and pressure variations obtained from Eqs. (1), (13), and (3) are

$$\frac{\rho}{\rho_0} = 1 + m_r\frac{t}{t_1}, \quad \frac{T}{T_0} = \frac{1 + \gamma^0 m_r\frac{T_i}{T_0}\frac{t}{t_1}}{1 + m_r\frac{t}{t_1}}, \quad \frac{p}{P_0} = 1 + \gamma^0 m_r\frac{T_i}{T_0}\frac{t}{t_1}, \quad 0 \le t < t_1 \tag{14}$$

$$\frac{\rho}{\rho_0} = 1 + m_r, \quad \frac{T}{T_0} = \frac{1 + \gamma^0 m_r\frac{T_i}{T_0}}{1 + m_r}, \quad \frac{p}{P_0} = 1 + \gamma^0 m_r\frac{T_i}{T_0}, \quad t_1 \le t < t_2 \tag{15}$$

$$\frac{\rho}{\rho_0} = 1 + m_r\frac{t_3 - t}{t_3 - t_2}, \quad \frac{T}{T_0} = \frac{1 + \gamma^0 m_r\frac{T_i}{T_0}}{1 + m_r} \times \left(1 - \frac{m_r}{1 + m_r}\frac{t - t_2}{t_3 - t_2}\right)^{\gamma^0 - 1}, \quad \frac{p}{P_0} = \left(1 + \gamma^0 m_r\frac{T_i}{T_0}\right)\left(1 - \frac{m_r}{1 + m_r}\frac{t - t_2}{t_3 - t_2}\right)^{\gamma^0}, \quad t_2 \le t < t_3 \tag{16}$$

$$\frac{\rho}{\rho_0} = 1, \quad \frac{T}{T_0} = \frac{1 + \gamma^0 m_r\frac{T_i}{T_0}}{(1 + m_r)^{\gamma^0}}, \quad \frac{p}{P_0} = \frac{1 + \gamma^0 m_r\frac{T_i}{T_0}}{(1 + m_r)^{\gamma^0}}, \quad t_3 \le t \le t_p \tag{17}$$

where ρ_0 is the initial density of the air within the cavern (at temperature T_0 and pressure P_0), γ^0 the ratio of the specific heats, and m_r the ratio of the injected to the initial cavern air mass

$$\gamma^0 = \frac{c_{p0}^0}{c_{v0}^0}, \quad m_r = \frac{\dot{m}_c t_1}{\rho_0 V} \tag{18}$$

Consider a series of charge/discharge cycles beginning at T_0 and P_0 in the first cycle. The first cycle state variations are given by Eqs. (14)–(17). The variations at subsequent cycles can be determined from the same equations, simply by substituting the prior cycle end variables as initial conditions for the current cycle. Being interested in the minima and maxima, the temperature and pressure at the end of each mode of charge/discharge as a function of the cycle number are as follows:

$$\frac{T_{n,\min}}{T_0} = \frac{p_{n,\min}}{P_0} = \frac{1 + \gamma^0 m_r \dfrac{T_i}{T_0} \displaystyle\sum_{j=0}^{n-1} (1+m_r)^{\gamma^0 j}}{(1+m_r)^{\gamma^0 n}}$$
$$= (1+m_r)^{-\gamma^0 n} + \gamma^0 m_r \frac{T_i}{T_0} \frac{1-(1+m_r)^{-\gamma^0 n}}{(1+m_r)^{\gamma^0} - 1} \tag{19}$$

$$\frac{T_{n,\max}}{T_0} = (1+m_r)^{\gamma^0 - 1} \frac{T_{n,\min}}{T_0}, \quad \frac{p_{n,\max}}{P_0} = (1+m_r)^{\gamma^0} \frac{p_{n,\min}}{P_0} \tag{20}$$

$T_{n,\max}$ and $p_{n,\max}$ are the temperature and pressure at the end of the nth charging cycle, and $T_{n,\min}$ and $p_{n,\min}$ at the end of the nth discharge cycle. Note that $T_{n,\min}$ and $p_{n,\min}$ are not necessarily the cycle minimum temperature and pressure, since the temperature and pressure at the discharge-mode end can be larger than the initial temperature and pressure of that cycle (see Fig. 3(*b*)). However, when steady periodic variations are reached, the initial and end states of all cycles are identical, and indeed $T_{n,\min}$ and $p_{n,\min}$ are the minima.

The variations of the cavern maximum and minimum temperatures as functions of the cycle number are shown in Fig. 3. As aforementioned, the cycles minimum and maximum temperatures can either decrease with time (Fig. 3(*a*)) or increase with time (Fig. 3(*b*)), depending on the values of m_r and T_i/T_0. In principle, the total energy added to the cavern air during the charging phase is $\dot{m}_c t_1 h_i = \dot{m}_c t_1 c_{p0}^0 T_i$. When the cavern air loses less energy (than $\dot{m}_c t_1 c_p T_i$) during the discharge phase, the cavern temperature increases, whereas if it loses more energy, the cavern temperature decreases. Eventually, at steady periodic variations, the cavern energy changes during discharge and charging phases become equal.

It is seen in the figure that the maximum and minimum temperatures approach asymptotically their limits (dashed horizontal lines). The asymptotic values can be obtained from the limits of Eqs. (19) and (20) at $n \to \infty$, which are

$$\frac{T_{s,\min}}{T_0} = \lim_{n\to\infty} \frac{T_{n,\min}}{T_0} = \frac{\gamma^0 m_r T_i/T_0}{(1+m_r)^{\gamma^0} - 1}, \quad \frac{T_{s,\max}}{T_0} = \lim_{n\to\infty} \frac{T_{n,\max}}{T_0}$$
$$= \frac{T_{s,\min}}{T_0} (1+m_r)^{\gamma^0 - 1} \tag{21}$$

$$\frac{p_{s,\min}}{P_0} = \lim_{n\to\infty} \frac{p_{n,\min}}{P_0} = \frac{\gamma^0 m_r T_i/T_0}{(1+m_r)^{\gamma^0} - 1}, \quad \frac{p_{s,\max}}{P_0} = \lim_{n\to\infty} \frac{p_{n,\max}}{P_0}$$
$$= \frac{p_{s,\min}}{P_0} (1+m_r)^{\gamma^0} \tag{22}$$

The subscript s indicates steady periodic conditions. Note that the asymptotic values can also be found directly by substituting $T = T_0 = T_{s,\min}$ in Eq. (17) and solving for $T_{s,\min}$. The maximum temperature can then be found by setting $T = T_{s,\max}$ and $T_0 = T_{s,\min}$ in Eq. (15). It is seen from the solutions that theoretically $0 \le T_{s,\min} \le T_i$, and $T_i \le T_{s,\max} \le \gamma^0 T_i$, where for $m_r \to 0$ $T_{s,\min} = T_{s,\max} = T_i$, and for $m_r \to \infty$ $T_{s,\min} = 0$ and $T_{s,\max} = \gamma^0 T_i$. If m_r is substituted from Eq. (22) into Eq. (21), then the asymptotic temperatures are obtain in terms of the asymptotic pressures and are as follows:

$$\frac{T_{s,\min}}{T_0} = \frac{\gamma^0 p_{s,\min}}{p_{s,\max} - p_{s,\min}} \frac{T_i/T_0}{} \left\{ \left(\frac{p_{s,\max}}{p_{s,\min}} \right)^{1/\gamma^0} - 1 \right\},$$
$$\frac{T_{s,\max}}{T_0} = \frac{\gamma^0 p_{s,\max}}{p_{s,\max} - p_{s,\min}} \frac{T_i/T_0}{} \left\{ 1 - \left(\frac{p_{s,\min}}{p_{s,\max}} \right)^{1/\gamma^0} \right\} \tag{23}$$

This result matches the solution of Osterle [8], obtained for $T_i = T_0$. Note that Osterle studied the case in which the cavern air is pressurized from a minimum pressure to a maximum pressure, and then depressurized back to the same minimum pressure. Thus, the pressures of each cycle are identical, while the amount of stored air varies. In the current study, the same amount of air is injected and withdrawn in each cycle and thus the pressure varies from cycle to cycle. However, at steady periodic conditions, the two cases coincide and the asymptotic temperatures are identical (the detailed thermodynamic paths lose their relevance).

It is seen from the solution that the pressure ratio is much larger than the temperature ratio (maximum to minimum). Notice that

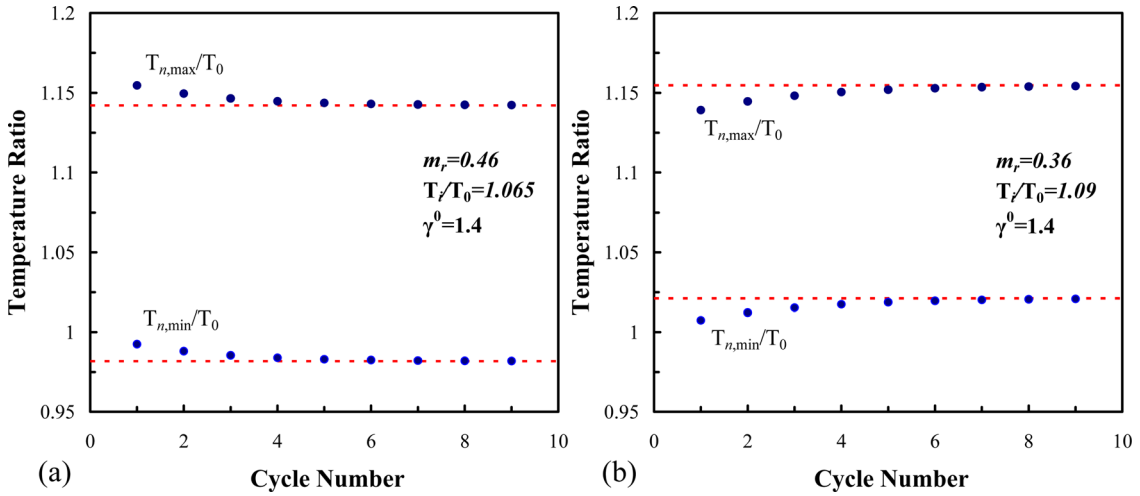

Fig. 3 Maximum and minimum cavern temperature variation dependence on the cycles progression. (*a*) For $m_r = 0.46$ and $T_i/T_0 = 1.065$; (*b*) for $m_r = 0.36$ and $T_i/T_0 = 1.09$. (The dashed lines represent the steady periodic temperature ratios)

those ratios depend only on m_r (assuming that $\gamma^0 = 1.4$ for T_0). Consider the example where $m_r = 0.336$, the pressure ratio is 1.5, whereas the temperature ratio is only 1.12. Therefore, substantial pressure ratios would entail only moderate temperature variations, even for adiabatic conditions.

The steady periodic air temperature and pressure variations can be obtained by replacing T_0 and P_0 by $T_{s,\min}$ and $p_{s,\min}$ in Eqs. (14)–(17). The solution is then written as follows:

$$\frac{T_s}{T_{s,\min}} = \frac{1 + \left[(1+m_r)^{\gamma^0} - 1\right]\frac{t}{t_1}}{1 + m_r \frac{t}{t_1}}, \qquad \frac{p_s}{p_{s,\min}} = 1 + \left[(1+m_r)^{\gamma^0} - 1\right]\frac{t}{t_1}, \quad 0 \le t < t_1 \tag{24}$$

$$\frac{T_s}{T_{s,\min}} = (1+m_r)^{\gamma^0 - 1}, \quad \frac{p_s}{p_{s,\min}} = (1+m_r)^{\gamma^0}, \quad t_1 \le t < t_2 \tag{25}$$

$$\frac{T_s}{T_{s,\min}} = \left(1 + m_r \frac{t_3 - t}{t_3 - t_2}\right)^{\gamma^0 - 1}, \quad \frac{p_s}{p_{s,\min}} = \left(1 + m_r \frac{t_3 - t}{t_3 - t_2}\right)^{\gamma^0}, \quad t_2 \le t < t_3 \tag{26}$$

$$\frac{T_s}{T_{s,\min}} = 1, \quad \frac{p_s}{p_{s,\min}} = 1, \quad t_3 \le t \le t_p \tag{27}$$

where t is the elapsed time from the beginning of the cycle, and

$$T_{s,\min} = \frac{\gamma^0 m_r T_i}{(1+m_r)^{\gamma^0} - 1}, \quad p_{s,\min} = \frac{P_0}{T_0}\frac{\gamma^0 m_r T_i}{(1+m_r)^{\gamma^0} - 1} \tag{28}$$

Since the discharge stage is isentropic (as modeled), at the steady periodic conditions, the specific entropy of the beginning and end of the charging stage should also be identical. Thus, the pressure and temperature of the air at the compression stage end are calculated by the isentropic ideal gas relations, as seen from Eq. (25) ($1+m_r$, is the maximum to minimum density ratio of the air).

The cycle maximum and minimum air pressures affect the required storage volume. In principle, the storage cavern operates between a minimum pressure (that provides the required turbine inlet pressure) and a maximum pressure (smaller than the cavern threshold pressure). For a given set of conditions, namely: rock temperature T_0, maximum and minimum cavern pressures, inlet air temperature T_i, and amount of injected air ($\dot{m}_c t_1$); the required cavern volume and initial pressure P_0 are derived from Eq. (22)

$$V = \frac{\dot{m}_c t_1 \gamma^0 \mathbf{R} T_i}{p_{s,\max} - p_{s,\min}}, \quad P_0 = \frac{p_{s,\max} - p_{s,\min}}{\gamma^0 \frac{T_i}{T_0}\left\{\left(\frac{p_{s,\max}}{p_{s,\min}}\right)^{1/\gamma^0} - 1\right\}} \tag{29}$$

A cavern volume of V which is filled initially with pressure P_0 is sufficient to accommodate the required CAES operating conditions.

3.2 Real Gas Model

3.2.1 Simplified Real Gas Model. A more realistic model would be to treat the air as a real gas. In this section, this is done with some simplification. Inspection of the thermodynamic properties of air reveals that the compressibility factor, the specific heats, and the internal energy derivative vary little within the expected cycle ranges of the temperature and pressure (see Table 1). Therefore, it is reasonable to assign a constant value to each of these variables, namely

$$\mathbf{Z} \approx \mathbf{Z}_0, \quad c_v \approx c_{v0}, \quad h_i - h = \int_T^{T_i} c_p dT \approx c_{p0}(T_i - T),$$
$$\left(\frac{\partial u}{\partial \rho}\right)_T = -\frac{\mathbf{R}T^2}{\rho}\left(\frac{\partial \mathbf{Z}}{\partial T}\right)_\rho \approx -\frac{\mathbf{R}T_0^2 \mathbf{Z}_{T0}}{\rho_0} \tag{30}$$

$\mathbf{Z}_0$, c_{v0}, c_{p0}, and $\mathbf{Z}_{T0}$ are all evaluate at the initial state condition (ρ_0, T_0), where $\mathbf{Z}_{T0}$ denotes the derivative of $\mathbf{Z}$ with respect to T. The substitution of the above approximations into Eq. (7) yields

$$\frac{V\rho c_{v0}}{\dot{m}_c}\frac{dT}{dt} = F_i(t)\left(c_{p0}(T_i - T) + \mathbf{Z}_0\mathbf{R}T + \frac{\mathbf{R}T_0^2\mathbf{Z}_{T0}}{\rho_0}\rho + g\Delta z\right) + F_e(t)\left(\mathbf{Z}_0\mathbf{R}T + \frac{\mathbf{R}T_0^2\mathbf{Z}_{T0}}{\rho_0}\rho + g\Delta z\right) \tag{31}$$

The kinetic energy term of Eq. (7) was neglected, but the potential energy term was kept to examine its influence at cases of tall caverns. Although Eq. (31) is more complex than the one for an ideal gas, it remains linear and can be solved analytically for the cavern air temperature. The first cycle density and temperature variations in the cavern obtained from Eqs. (1) and (31) are

$$\frac{\rho}{\rho_0} = 1 + m_r\frac{t}{t_1}, \quad T = c_1 + c_2\frac{\rho}{\rho_0} + (T_0 - c_1 - c_2)\frac{\rho}{\rho_0}^{-(\gamma - R^*)}, \quad 0 \le t < t_1 \tag{32}$$

$$\frac{\rho}{\rho_0} = 1 + m_r, \quad T = (c_1 + c_2)\left(1 - (1+m_r)^{-(\gamma - R^*)}\right) + c_2 m_r + T_0(1+m_r)^{-(\gamma - R^*)}, \quad t_1 \le t < t_2 \tag{33}$$

$$\frac{\rho}{\rho_0} = 1 + m_r\frac{t_3 - t}{t_3 - t_2}, T = \left(T(t_2) + c_3 - c_4(1+m_r)\right) \times \left(\frac{\rho/\rho_0}{1+m_r}\right)^{R^*} - c_3 + c_4\frac{\rho}{\rho_0}, \quad t_2 \le t < t_3 \tag{34}$$

$$\frac{\rho}{\rho_0} = 1, \quad T = \left(T(t_2) + c_3 - c_4(1+m_r)\right)(1+m_r)^{-R^*} - c_3 + c_4, \quad t_3 \le t \le t_p \tag{35}$$

where

Table 1 Representative ranges of cavern design parameters and initial thermodynamic conditions

Variable	Definitions	Minimum value	Maximum value	Units	Comments
T_0	Rock temperature	20	60	°C	Data from Refs. [12,13]
T_i/T_0	Relative inlet air temperature	1	1.2	—	
$p_{s,\min}$	Minimum cavern operational pressure	20	70	bar	According to the desired turbine inlet pressure
$p_{s,\max}/p_{s,\min}$	Cycle cavern pressure ratio	1.2	1.8	—	From economical consideration (see Fig. 8)
P_0	First fill cavern pressure	17	77	bar	Based on Eq. (29)
m_r	Injected to initial air mass ratio	0.15	0.55	—	Based on Eq. (22)

$$c_1 = \frac{c_{p0}T_i + g\Delta z}{c_{p0} - \mathbf{R}\mathbf{Z}_0}, \quad c_2 = \frac{\mathbf{R}T_0^2\mathbf{Z}_{T0}}{c_{p0} - \mathbf{R}\mathbf{Z}_0 + c_{v0}}, \quad c_3 = \frac{g\Delta z}{\mathbf{R}\mathbf{Z}_0},$$
$$c_4 = \frac{\mathbf{R}T_0^2\mathbf{Z}_{T0}}{c_{v0} - \mathbf{R}\mathbf{Z}_0}, \quad \gamma = \frac{c_{p0}}{c_{v0}}, \quad R^* = \frac{\mathbf{R}\mathbf{Z}_0}{c_{v0}} \tag{36}$$

The temperature solution is based on a constant compressibility factor ($\mathbf{Z}_0$) assumption. However, to improve the air pressure calculation accuracy, the instantaneous compressibility factor can be used in Eq. (3).

As previously, consider a series of charge/discharge cycles beginning with T_0 and P_0 at the first cycle. The first cycle conditions are given by Eqs. (32)–(35), whereas subsequent cycle conditions can be found by substituting the appropriate initial conditions in Eqs. (32)–(35). Eventually, steady periodic conditions will be reached. They can be found by setting $T = T_0 = T_{s,\min}$ in Eq. (35) and solving for $T_{s,\min}$, which in turn can be substituted in Eq. (33) to obtain $T_{s,\max}$. The resulting minima and maxima conditions are

$$T_{s,\min} = \frac{(c_1 + c_3 + (c_2 - c_4)(1+m_r))(1+m_r)^{-R^*+\gamma} - (c_3 - c_4)(1+m_r)^{\gamma} - (c_1 + c_2)}{(1+m_r)^{\gamma} - 1},$$
$$T_{s,\max} = \frac{(c_1 + c_2(1+m_r))(1+m_r)^{\gamma} - (c_1 + c_2 + c_3 - c_4)(1+m_r)^{R^*} + c_3 - c_4(1+m_r)}{(1+m_r)^{\gamma} - 1} \tag{37}$$

$$\frac{p_{s,\min}}{P_0} = \frac{\mathbf{Z}_{\min}}{\mathbf{Z}_0}\frac{T_{s,\min}}{T_0}, \quad \frac{p_{s,\max}}{P_0} = (1+m_r)\frac{\mathbf{Z}_{\max}}{\mathbf{Z}_0}\frac{T_{s,\max}}{T_0} \tag{38}$$

where $\mathbf{Z}_{\min} = \mathbf{Z}(\rho_0, T_{s,\min})$, and $\mathbf{Z}_{\max} = \mathbf{Z}(\rho_0(1+m_r), T_{s,\max})$. At the limiting case of $m_r \to 0$, Eq. (37) reduce to $T_{s,\min} = T_{s,\max} = T_i$, as for the ideal gas model. The steady periodic temperature variations of the air cavern can be calculated by setting $T = T_s$, and $T_0 = T_{s,\min}$ in Eqs. (32)–(35). The pressure is then obtained from Eq. (3) with $p = p_s$ and $T = T_s$.

The required storage volume and the initial fill pressure P_0 can again be calculated from Eq. (38), for the given set of: maximum and minimum cavern pressure, rock mass temperature T_0, inlet air temperature T_i, and amount of injected air ($\dot{m}_c t_1$). The storage volume cannot be found analytically, and Eq. (38) must be solved numerically.

3.2.2 Complex Real Gas Model. The "complex" model refers to a real gas with its thermodynamic property fully dependent on temperature and density. The adopted representation of the

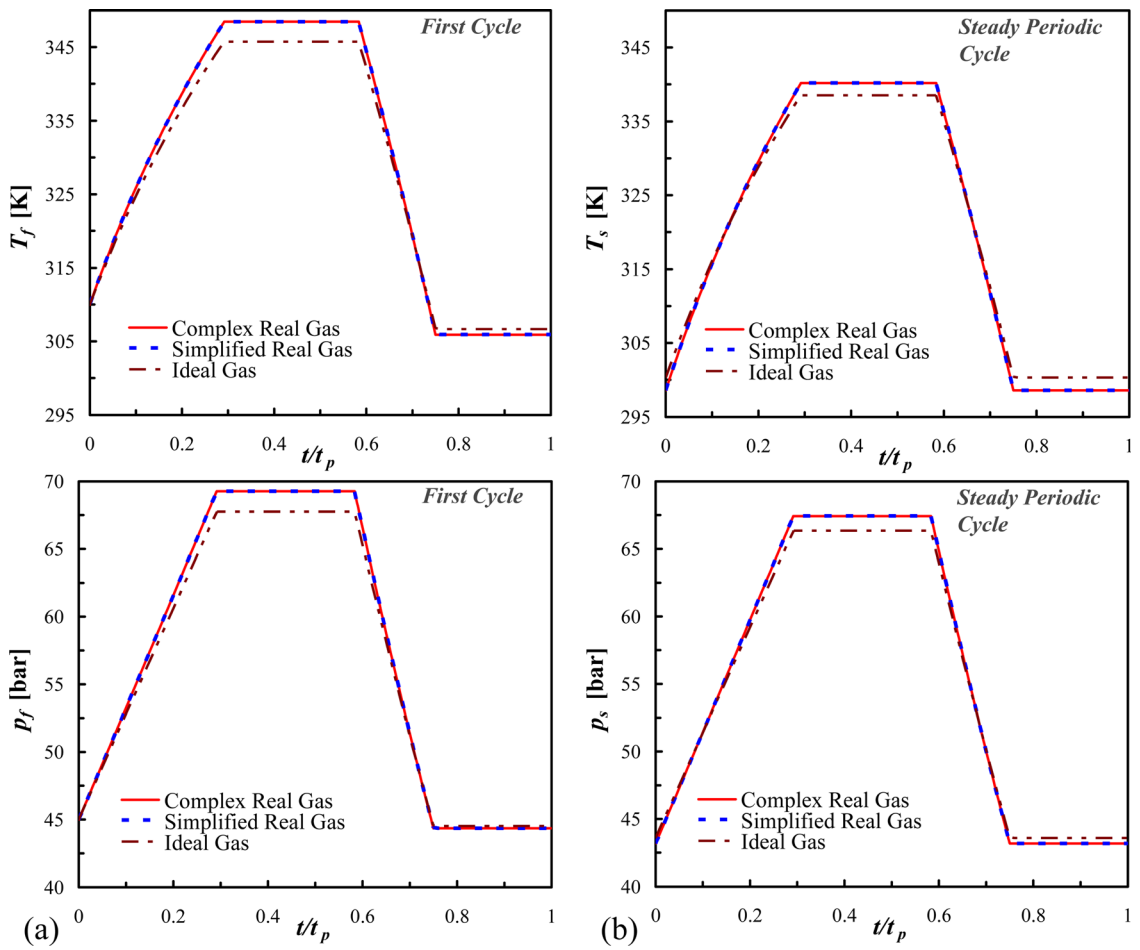

Fig. 4 Temperature and pressure variations of the cavern air for $T_0 = 310$ K, $P_0 = 45$ bar, $T_i = 320$ K, $m_r = 0.35$, $t_1/t_p = 7/24$, $t_2/t_p = 14/24$, $t_3/t_p = 18/24$. (*a*) During the first cycle; (*b*) during a steady periodic cycle.

Table 2 Relative deviations of the predicted temperatures and pressures from the complex real gas model predictions (in percents) for the conditions of Fig. 4

Model	$T_{s,\max}$	$T_{s,\max}/T_{s,\min}$	$T_{s,\max}-T_{s,\min}$	$p_{s,\max}$	$p_{s,\max}/p_{s,\min}$	$p_{s,\max}-p_{s,\min}$
Ideal gas	0.47	1.04	7.98	1.6	2.54	6.16
Simplified real gas	0.01	0.01	0.11	0.02	0.02	0.04

properties follows the Sychev et al. [10] model. The representation is exceptionally accurate for air within a temperature range from 70 to 1500 K, and pressures from 0.01 to 100 MPa. It was selected owing to its simple expression and accuracy. Accordingly, the compressibility factor and the ideal gas specific heat are

$$\mathbf{Z} = 1 + \sum_{i=1}^{8}\sum_{j=0}^{S_i} b_{ij}\frac{\rho_r^i}{T_r^j} \tag{39}$$

$$\frac{c_p^0}{\mathbf{R}} = \sum_{j=0}^{6}\alpha_j\left(\frac{T}{T_{\text{ref}}}\right)^j + \sum_{j=1}^{6}\beta_j\left(\frac{T}{T_{\text{ref}}}\right)^{-j} \tag{40}$$

where $\rho_r = \rho/\rho_{cr}$ and $T_r = T/T_{cr}$, with ρ_{cr} and T_{cr} being the air density and temperature at the critical point, $T_{\text{ref}} = 100$ K, and b_{ij}, α_j, and β_j are constant coefficients. Following Eq. (7), the air temperature within the cavern can be calculated by the differential-algebraic equations (DAE)

$$\frac{V\rho c_v(\rho,T)}{\dot{m}_c}\frac{dT}{dt} = F_i(t)\left(h_i(\rho_i,T_i) - h(\rho,T) + \mathbf{Z}(\rho,T)\mathbf{R}T - \rho\frac{\partial u}{\partial\rho}(\rho,T) + g\Delta z\right) + F_e(t)\left(\mathbf{Z}(\rho,T)\mathbf{R}T - \rho\frac{\partial u}{\partial\rho}(\rho,T) + g\Delta z\right) \tag{41}$$

$$\mathbf{Z}(\rho_i,T_i)\rho_i T_i = \mathbf{Z}(\rho,T)\rho T \tag{42}$$

where c_v, h, and $\partial u/\partial\rho$ are obtained from Eqs. (8)–(10). The air density entering the cavern, ρ_i, is another unknown to be calculated by Eq. (42) that equates the inlet air and the cavern air pressures. The temperature solution and Eq. (3) yield the cavern air pressure.

Equations (41) and (42) were solved numerically by Maple [11] based on the *rosenbrock_dae* code, which is an extension of the *rosenbrock* code to solutions of DAE problems (an implicit Rosenbrock third-fourth order Runge–Kutta method). The numerical computation was verified for the discharge stage, which is isentropic, and can be obtained from the algebraic equation

$$s(\rho_{\max},T_{\max}) - s(\rho,T) = 0 \tag{43}$$

where s is the air entropy (calculated from thermodynamic relations [10]), $\rho_{\max}$ and $T_{\max}$ are the air density and temperature at the beginning of the discharge stage. Expectedly, the numerical values of the temperature obtained by Eq. (43) coincide with the numerical solution of Eq. (41), during discharge.

4 Results and Discussion

The analysis reveals that at adiabatic conditions, the cavern minima and maxima of the temperature and pressure depend on: the cavern-air initial thermodynamic state, the inlet air temperature, and the injected to initial cavern air mass ratio. Realistic ranges of these parameters are listed in Table 1. The initial cavern air temperature is equal to the local surrounding rock temperature. The initial air pressure and the injected to initial air mass ratio are determined so as to provide the desired operational cavern maximum and minimum pressures.

It is noted that for a given condition set (namely, P_0, T_0, V, $\dot{m}_c t_1$) the value of $m_r = \dot{m}_c t_1/V\rho_0$ calculated by the ideal gas model is slightly different than the one calculated by the other two models, obviously from the differences of ρ_0 ($\rho_0 = P_0/\mathbf{R}T_0$ for ideal gas, and $\rho_0 = P_0/\mathbf{Z}_0\mathbf{R}T_0$ for real gas). In Secs. 4.1 and 4.2, whenever m_r is provided it refers to the "exact" calculation.

4.1 Cavern Temperature and Pressure. The first and the steady periodic cycle temperature and pressure distributions, calculated by each of the three models, are illustrated in Figs. 4(*a*) and 4(*b*) (for the indicated set of conditions). Note that for the adiabatic case the storage duration periods bear no effect on the cavern condition and can be omitted from the graphical representation. Nonetheless, the storage periods are provided throughout the work for

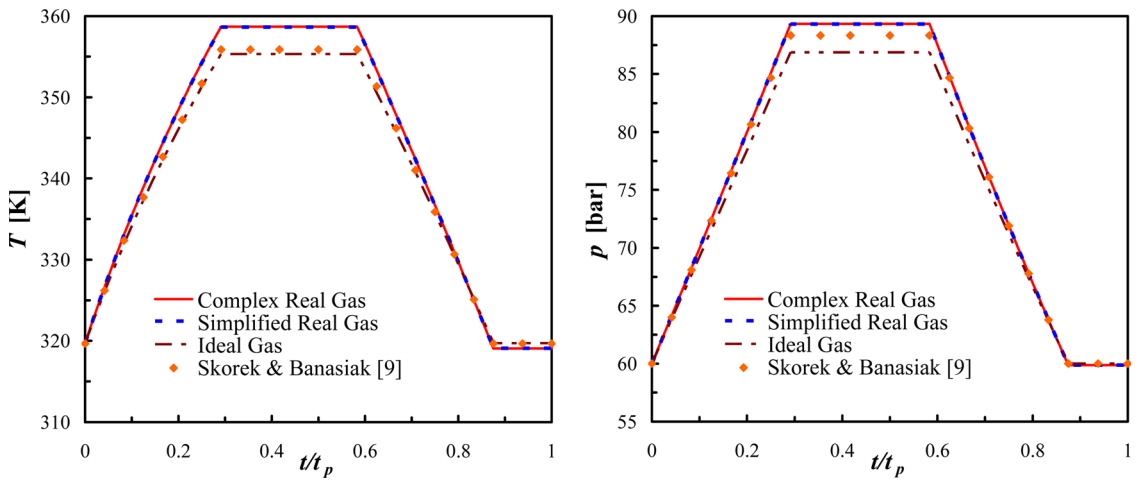

Fig. 5 Comparison of the calculated air temperature and pressure variations during a cycle for different thermodynamic models. $T_0 = 319.7$ K, $P_0 = 60$ bar, $T_i = 338$ K, $V = 300{,}000$ m^3, $\dot{m}_c = 236$ kg/s, $t_1 = 7$ h, $t_2 = 14$ h, $t_3 = 21$ h, $t_p = 24$ h.

Table 3 Relative deviations of the predicted temperatures and pressures from the complex real gas model predictions (in percents) for the conditions of Fig. 5

Model	$T_{s,max}$	$T_{s,max}-T_{s,min}$	$p_{s,max}$	$p_{s,max}-p_{s,min}$
Ideal gas	0.94	8.66	2.75	8.38
Semi-ideal gas [9]	0.79	7.16	1.12	3.41
Simplified real gas	0.016	0.146	0.018	0.055

consistency with other representations. Evidently, an excellent agreement exists between the simplified and the complex gas model solutions, while the ideal gas model exhibits slight deviations. Those are mainly attributed to the term $\rho(\partial u/\partial\rho)_T$ which equals zero for an ideal gas. Consequently, the ideal gas model predicts milder temperature gradients during both charging and discharge stages and thereby reduces the temperature fluctuations. The calculated temperature and pressure ratios ($T_{s,max}/T_{s,min}$, and $p_{s,max}/p_{s,min}$) are 1.14 and 1.562, respectively, for the complex model (and the simplified real gas model), and 1.128 and 1.522 for the ideal gas model. The relative deviations of the simplified models from the complex model results are presented in Table 2. Overall, for the conditions described in the figure, the ideal gas model suffices to predict reasonably well the temperature and pressure changes in the cavern.

In order to compare the results against published calculations of Skorek and Banasiak [9], the cavern temperature and pressure variations for a full cycle span were calculated with the three models for conditions identical to those used by Skorek and Banasiak. In the calculations, Skorek and Banasiak neglected the heat exchange between the air and the reservoir walls, and considered the air to be a semi-ideal gas. As observed in Fig. 5, the results of the semi-ideal gas model [9] falls well within the range of the ideal gas and the complex model predictions, as expected. The relative deviation of the simplified models from the complex model results is presented in Table 3. Again, the simplified real gas model is in excellent agreement with the complex model, while the semi-ideal and ideal gas models exhibit smaller temperature and pressure fluctuations.

Obviously, the temperature and pressure fluctuation amplitudes in the cavern depend primarily on m_r. In general, a larger value of m_r induces larger changes of the density, temperature, and pressure. This assertion is seen in Fig. 6, when the cavern temperature and pressure ratios are plotted against m_r. As observed, it is also seen that results of the simplified real gas representation and of the complex model are in excellent agreement even for cases of larger than normal pressure ratios. In fact, the error between the two models becomes perceptible only at impractical high value of m_r (the practical limit of m_r appears in Table 1). As previously mentioned, the ideal gas model yields

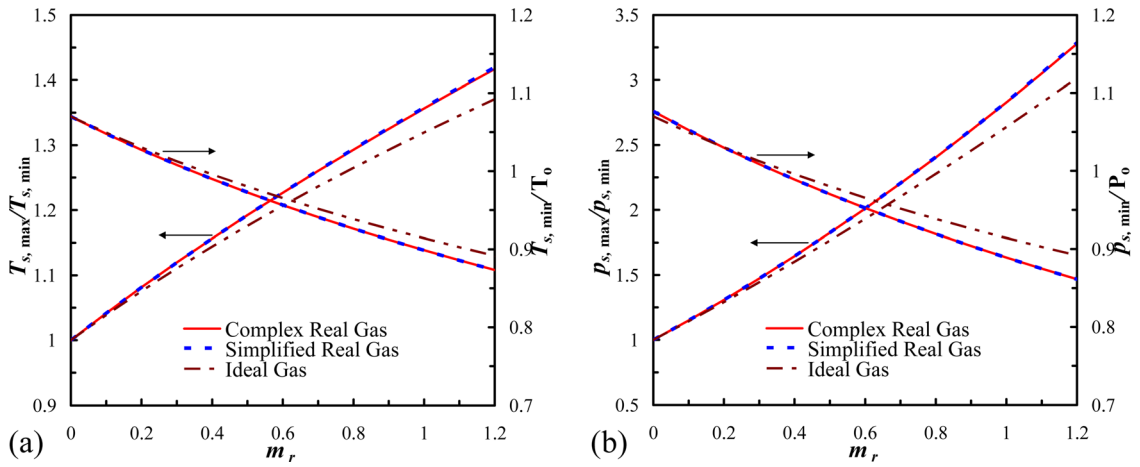

Fig. 6 Effects of m_r on the cavern temperature ratios (*a*) and pressure ratios (*b*), for $T_0 = 300$ K, $P_0 = 40$ bar, $T_i/T_0 = 1.07$

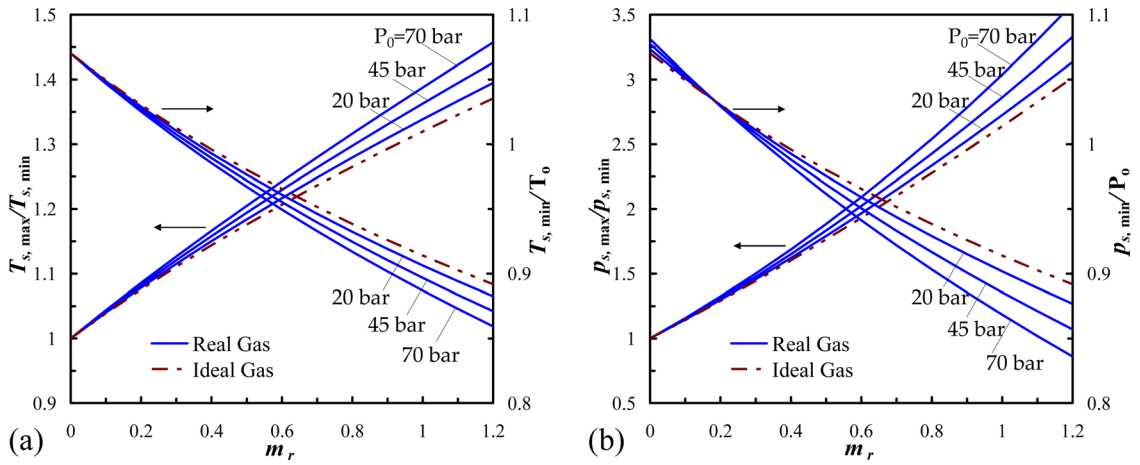

Fig. 7 Effects of m_r on the cavern temperature ratios (*a*) and pressure ratios (*b*), for $T_0 = 300$ K, $T_i/T_0 = 1.07$, and at different P_0's

Table 4 Dependence of the air pressure ratios on the cavern height for $P_0 = 40$ bar, $T_0 = 300$ K, $T_i/T_0 = 1.07$, and $m_r = 0.4$. (The calculations were preformed by Eq. (38))

Δz (m)	$p_{s,\max}/P_0$	Relative error (%)	$p_{s,\max}/p_{s,\min}$	Relative error (%)
0	1.6269	0	1.6450	0
50	1.6274	0.03	1.6463	0.08
100	1.6280	0.07	1.6476	0.16
150	1.6286	0.10	1.6489	0.24

smaller changes of temperature and pressure. The deviation in temperature and pressure increases at larger m_r's and is mainly caused by the term $\rho(\partial u/\partial\rho)_T$ which becomes more dominant (for ideal gas the latter vanishes).

For an ideal gas, the maximum to minimum ratios of the temperature and pressure depend only on m_r (see Eq. (25)). For a real gas, these ratios depend also on the initial air state and the inlet air temperatures. Within the ranges listed in Table 1, T_0 and T_i have a negligible effect on these ratios. Thus, the differences between ideal gas and real gas, seen in Fig. 6, are expected to depend only on P_0. That dependence is depicted in Fig. 7, where the temperature and pressure ratios are presented for different values of P_0. As expected, the deviation of a real gas from an ideal gas behavior is larger at higher pressures (higher densities).

In conclusion, the computations reveal that for typical conditions of CAES plants, the temperature and pressure in the cavern can adequately be calculated by the simplified real gas model. It is also shown that for a real gas, the temperature and pressure ratios do not depend only on m_r (as for ideal gas) but also on the storage pressure. The deviation from an ideal gas behavior increases as the storage mean pressure and pressure fluctuations increase. However, for practical operating conditions, the relative errors are confined within few percent spans.

In all the above calculation, the potential energy term was neglected ($g\Delta z = 0$). To asses if it is indeed negligible, the air maximum pressure and pressure ratio were calculated (by Eq. (38)) for typical conditions and various cavern heights. Results of those calculations (see Table 4) show that the potential energy omission is justified.

4.2 Storage Volume. The storage volume of cavern reservoirs is a design parameter. In principle, the storage volume should be sufficiently large to store the required air mass and provide the desired turbine inlet pressures without exceeding the cavern threshold pressure. The minimal storage volume is the one that $p_{s,\max}$ reaches the cavern threshold pressure. Obviously, the reservoir can operate with smaller pressure ratios (smaller $p_{s,\max}$'s), which would require larger storage volumes. The interrelationship of the storage pressure ratio to the required storage volume is demonstrated in Fig. 8 in a dimensionless form. As observed, the storage pressure ratio has a dominant effect on the storage volume. At small pressure ratios, a slight increase of the ratio substantially decreases the storage volume and its cost, but increases both, the required compression work and compressor cost. On the other hand, at large pressure ratios, a decrease of the ratios do not affect much the storage volume and reduces the required compression work and compressor cost. Consequently, the selection of the storage pressure ratio and its corresponding storage volume should be based on both design considerations and economical criteria and should be preferably in between 1.2 and 1.8. For demonstration, consider the Huntorf plant caverns that have a threshold pressure of 100 bar [3]. Technically, the caverns can operate with a pressure ratio grater than 2 (and smaller caverns), but actually operate with a pressure ratio of about 1.4.

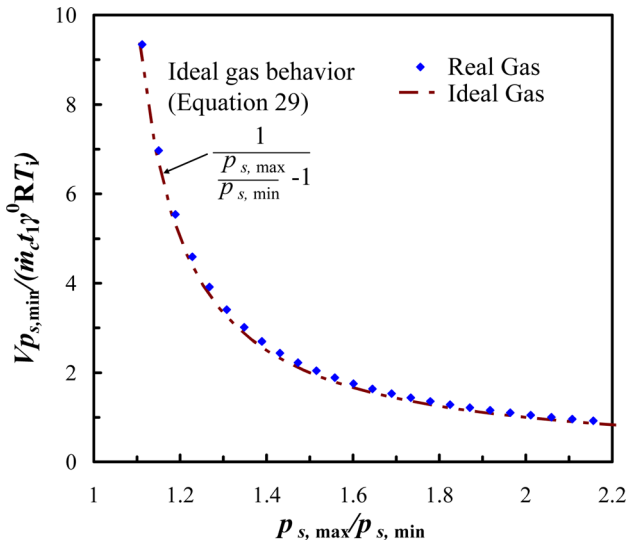

Fig. 8 The dimensionless storage volume dependence on the storage pressure ratio for $T_0 = 300$ K, $P_0 = 40$ bar, $T_i/T_0 = 1.07$

For a given storage volume, real gas exhibits higher pressure fluctuations than those calculated under the assumption of ideal gas. Therefore, as seen in Fig. 8, the actually needed volumes are larger than those calculated for ideal gases. Those volume deviations are larger for both, higher storage mean pressures, and pressure ratios.

5 Conclusions

A theoretical investigation of adiabatic cavern response to the charge/discharge cycles of CAES plants was conducted. The analysis provides useful expressions for the periodic air temperature and pressure variations. It is demonstrated that the air thermodynamic properties can adequately be represented by a simplified real gas model, in contrast to an ideal gas model that yields smaller pressure fluctuations and storage volume requirements. It is also shown that the temperature and pressure ratios do not depend solely on the injected to initial cavern air mass ratio (as valid for ideal gases) but also on the storage mean pressure. The deviation from an ideal gas behavior increases as the storage mean pressure and pressure fluctuations increase, however, for practical conditions that deviation does not exceed few percents. It is evident from the results that the storage pressure ratio has a dominant effect on the required storage volume, and should be preferably in between 1.2 and 1.8. The precise value must be based on both design considerations and economical criteria. Additionally, the solutions can be used to estimate the compressor and turbine works, and the entire CAES plant performance.

Nomenclature

b_{ij} = constant coefficient
c_i = $i = 1,2,3,4$ coefficients defined in Eq. (36), K
c_v = constant-volume specific heat, kJ/(kg K)
c_p = constant-pressure specific heat, kJ/(kg K)
CD = charge/discharge time ratio
e = specific energy, kJ/kg
F_i, F_e = dimensionless functions defined in Eq. (5)
g = gravitational acceleration, m/s^2
h = specific enthalpy, kJ/kg
$\dot{m}_c$ = compressor mass flow rate, kg/s
m_r = injected to initial cavern air mass ratio, $\dot{m}_c t_1/(\rho_0 V)$
n = cycle number
p = pressure, kPa
P_0 = initial pressure, kPa
R = specific gas constant, kJ/(kg K)
R^* = dimensionless group, $\mathbf{RZ}_0/c_{v0}$
s = entropy, kJ/(kg K)
t = time, s
t_p = cycle time period, s

t_i = $i = 1,2,3$, process duration time, see Fig. 2, s
T = temperature, K
T_0 = initial temperature, K
T_i = injected air temperature, K
u = specific internal energy, kJ/kg
v = velocity, km/s
V = cavern volume, m^3
z = vertical coordinate, km
$\mathbf{Z}$ = compressibility factor
$\mathbf{Z}_T$ = derivative of $\mathbf{Z}$ with respect to T, K^{-1}

Greek Symbols

α_j, β_j = constant coefficients
γ = specific heat ratio at initial state, c_{p0}/c_{v0}
ρ = density, kg/m^3

Superscript

0 = ideal gas properties

Subscripts

0 = initial state
cr = critical
e = control volume outlet
f = first cycle
i = control volume inlet
r = reduced
ref = reference
s = steady periodic cycle

References

[1] Kushnir, R., Ullmann, A., and Dayan, A., 2008, "Steady Periodic Gas Flow Around a Well of a CAES Plant," Transp. Porous Media, **73**(1), pp. 1–20.
[2] Kushnir, R., Ullmann, A., and Dayan, A., 2010, "Compressed Air Flow Within Aquifer Reservoirs of CAES Plants," Transp. Porous Media, **81**(2), pp. 219–240.
[3] Crotogino, F., Mohmeyer, K. U., and Scharf, R., 2001, "Huntorf CAES: More than 20 Years of Successful Operation," Solution Mining Research Institute, Spring Meeting, Orlando, Florida.
[4] Nakhamkin, M., Andersson, L., Turpin, D., Howard, J., Meyer, R., Schainker, R., Pollak, R., and Mehta, B., 1992, "First U.S CAES Plant Initial Startup and Operation," *Proceedings of the 54th American Power Conference*, Illinois Institute of Technology, Chicago, IL, Vol. 54, pp. 154–161.
[5] Quast, P., and Crotogino, F., 1979, "Initial Experience with the Compressed-Air Energy Storage (CAES) Project of Nordwestdeutsche Kraftwerke AG (NWK) at Huntorf/West Germany," Erdoel-Erdgas-Z., **95**(9), pp. 310–314.
[6] Nakhamkin, M., Swensen, E., Schainker, R., and Mehta, B., 1989, "CAES Plant Performance and Economics as a Function of Underground Salt Dome Storage Transient Processes," ASME Paper No. 89-GT-143.
[7] Nakhamkin, M., Swensen, E., and Mehta, B., 1990, "Analysis of Temperature Transients of Underground Air Storage in a Salt Dome During CAES Plant Operation," Solution Mining Research Institute, Fall Meeting, Paris.
[8] Osterle, J. F., 1991, "The Thermodynamics of Compressed Air Exergy Storage," ASME J. Energy Resour. Technol., **113**(1), pp. 7–11.
[9] Skorek, J., and Banasiak, K., 2006, "Thermodynamic Analysis of the Compressed Air Energy Storage Systems Operation," Inzynieria Chemiczna I Procesowa, **27**, pp. 187–200.
[10] Sychev, V. V., Vasserman, A. A., Kozlov, A. D., Spiridonov, G. A., and Tsymarny, V. A., 1987, Thermodynamic Properties of Air, Hemisphere, Washington.
[11] Maplesoft, 2003, "Maple 9 Learning Guide," Waterloo Maple Inc., Waterloo, Canada.
[12] Allen, R. D., Doherty, T. J., and Fossum, A. F., 1982, "Geotechnical Issues and Guidelines for Storage of Compressed Air in Excavated Hard Rock Caverns," Pacific Northwest Laboratory, Technical Report No. PNL-4180.
[13] Allen, R. D., Doherty, T. J., and Thoms, R. L., 1982, "Geotechnical Issues and Guidelines for Storage of Compressed Air in Solution-Mined Salt Cavities," Pacific Northwest Laboratory, Technical Report No. PNL-4242.